CrossMark

ORIGINAL PAPER

Distinctive slit-shaped porous carbon encapsulating phosphorus as a promising anode material for lithium batteries

Jiaoyang Li[1] · Li Wang[1,2] · Yumei Ren[2] · Yong Zhang[3] ·
Youfu Wang[3] · Aiguo Hu[3] · Xiangming He[1,2]

Abstract A distinctive structure of carbon materials for Li-ion batteries is proposed for the preparation of red phosphorus-carbon composites. The slit-shaped porous carbon is observed with aggregation of plate-like particles, whose isotherm belongs to the H3 of type IV. The density functional theory (DFT) method reveals the presence of micro-mesopores in the 0.5–5 nm size range. The unique size distribution plays an important role in adsorbing phosphorus and electrochemical performance. The phosphorus-slit-shaped porous carbon composite shows initial capacity of 2588 mAh g^{-1}, reversible capacity of 1359 mAh g^{-1} at a current density of 100 mA g^{-1}. It shows an excellent coulombic efficiency of ~99 % after 50 cycles.

✉ Xiangming He
hexm@tsinghua.edu.cn

Aiguo Hu
hagmhsn@ecust.edu.cn

1 Institute of Nuclear and New Energy Technology, Tsinghua University, Beijing 100084, People's Republic of China

2 Jiangsu Huadong Institute of Li-ion Battery, Zhangjiagang, Jiangsu 215000, People's Republic of China

3 Shanghai Key Laboratory of Advanced Polymeric Materials, School of Materials Science and Engineering, East China University of Science and Technology, Shanghai 200237, People's Republic of China

1.Introduction

Lithium-ion rechargeable batteries are used as power sources for a wide variety of transportation, electric grid, and telecommunication. Nowadays, graphite (372 mAh g^{-1}) is generally used as an anode material for lithium ion batteries, but it cannot meet the demand of social development [1–4]. Much effort has focused on increasing the capacity and efficiency of materials for many decades. Lots of materials have been synthesized to increase the ability of reacting reversibly with large amounts of Li per formula unit, such as Sn-based oxide [5, 6], Si-based composites [7, 8], transition metal oxides [9, 10], metal nitrides [11, 12], and metal phosphide systems [13–15]. In addition, elemental phosphorus is another potentially attractive anode material based on the three electrons' reaction (3Li + P → Li_3P). The corresponding theoretical specific capacity is as high as 2595 mAh g^{-1} [16, 17]. Phosphorus shows three main allotropes: white, red, and black. Among these allotropes, red phosphorus is an abundant and eco-friendly material. However, because of its electronic insulation, the experimental capacity of red phosphorus is far from theoretical value and dramatically fading after a few cycles [16]. Much effort has been made to address these issues; one of the most important ways is to fabricate phosphorus-carbon composite [18, 19]. He and co-workers reported the benefit of nano-structured red phosphorus composite materials with porous carbon as the host material, an improvement of both high lithium storage capacity and stable cycling [18]. In such materials, the conductive porous carbon acted as framework can enhance the electrical conductivity of the composite materials. Although phosphorus is an electronic insulator, the composite still shows good performance. It can be attributed to the characteristics of porous carbon. High specific surface area, low electrical resistivity, and porous structure allow good electrolyte accessibility through the

🍂 Springer

electrode. These characteristics motivate us to explore the improvement of electrochemical properties of phosphorus composite with special pore structured carbon materials.

Herein, we demonstrate a facile preparation of red phosphorus composite with slit-shaped porous carbon for lithium storage, which was used as an anode material. Particularly, the slit-shaped porous carbon with unique size distribution contributes to load phosphorus and efficiently improve electrochemical properties. This composite shows a reversible capacity of 1359 mAh g^{-1} at a current density of 100 mA g^{-1}. It possesses prominent capacity retention of 60 % from the second cycle to 50th cycle and a high coulombic efficiency of ~99 %.

2. Experimental section

Synthesis of slit-shape carbon Formaldehyde dimethyl acetal was added to $FeCl_3$ in 1,2-dichloroethane. After degassing by nitrogen bubbling, the mixture was stirred at 45 °C for 5 h to build up the preliminary polymeric network and then heated at 80 °C for 19 h to complete the cross-linking. The resulting precipitate was washed three times with methanol and HCl, then Soxhlet extracted with methanol for 24 h, and finally dried under reduced pressure at 60 °C for 24 h. The slit-shaped carbon was obtained by carbonization [20].

Preparation of composites Red phosphorus was washed with distilled water to remove oxides before processing. Red phosphorus was put on the bottom of the stainless steel vessel, and slit-shaped carbon was put into a small beaker which was placed into the same stainless steel vessel. The vessel was sealed in an argon-filled glove box. Then, the vessel was heated at 450 °C for 3 h. The composite material was obtained by cooling the vessel to room temperature.

Characterization The TG measurement was carried out in argon flow at a heating rate of 10 °C min^{-1} using NETZSCH STA 449F3. X-ray diffraction (XRD) analysis was performed using a Rigaku D/max-2500 with filtered Cu Kα radiation. The microstructure of the red phosorus composite was characterized by scanning electron microscopy (SEM; JEOL-6301F).

The surface area and pore volume were measured by N_2 adsorption and desorption isotherms using a Quantachrome NOVA 2200 analyzer at −196 °C. All the samples were degassed at 150 °C on a vacuum line following a standard protocol before measurement. The total pore volume was calculated from the amount adsorbed at a relative pressure of 0.99. The surface area was calculated by Brunauer–Emmett–Teller (BET) method; the total pore volumes and micropore volumes were calculated by quenched solid density functional theory (QSDFT) method and the Dubinin Radushkevich (DR) method, respectively.
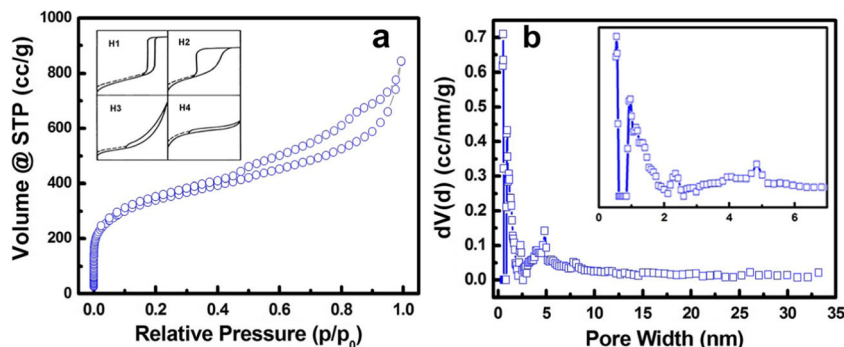
Electrochemical characterization Electrochemical measurements were performed using CR2032 coin-type cells assembled in an argon-filled glove box. The working electrodes were made by pressing a 0.8-cm^2 thin film (containing 70 wt% red phosphorus composite, 20 wt% acetylene black, 10 wt% polyacrylonitrile) onto Ni mesh. The electrodes were dried in a vacuum oven at 80 °C for 12 h before test. Electrochemical cells were assembled with the composite as cathode, metallic lithium disk as anode, and Celgard 2400 porous film as separator. The electrolyte used in this work is a mixed solvent of dimethylformamide (DMF) and 1,3-dioxolane (DOL) (1:1 by volume.). The charge–discharge experiments were performed galvanostatically with current density of 100 mA g^{-1} between 0 and 3 V on battery testers (Land CT2001A). The cells were cycled at room temperature.

3. Results and discussion

In this work, the porosity feature of the slit-shaped porous carbon sample was investigated by N_2 adsorption–desorption technique. The isotherms possess distinct adsorption and desorption branches, as shown in Fig. 1a, which belong to type IV profile in virtue of the International Union of Pure and Applied Chemistry (IUPAC) classification. More specially, it belongs to the H3 of type IV (the inset in Fig. 1a), different from the common H1. In detail, the type H3 loop, which does not exhibit any limiting adsorption at high p/p°, is observed with aggregates of plate-like particles giving rise to slit-shaped pores [21]. It is in accord with the SEM image of slit-shaped porous carbon which is shown in Fig. S1. In order to further analyze the pore structure of carbon, the pore size distributions of the micro-mesopore size distribution of the slit-shaped porous carbon were calculated by the QSDFT kernel from the N_2 adsorption (Fig. 1b), assuming a slit pore geometry for micro-mesopores. The analysis reveals the presence of micro-mesopores in the 0.5–5 nm size range, which can be acted as phosphide reservoirs to alleviate the loss of phosphorus [22]. Furthermore, the micropore volumes calculated from N_2 isotherms by the Dubinin Radushkevich (DR) method indicate that the carbon possesses narrow microporosity [23]. The BET surface area, density functional theory (DFT) pore volume, and micropore volume are given in Table 1, and volume histogram is shown in Fig. S2. Clearly, the micropore volume accounted for 38.3 % of total pore volume.

The phosphorus-carbon composite (P@C) was prepared by a vaporization/adsorption strategy. X-ray diffraction (XRD) patterns of red phosphorus, slit-shaped porous carbon, and P@C are presented in Fig. 2. The XRD pattern shows that the starting red phosphorus powder has a medium-range

ordered structure with its first sharp diffraction peak (FSDP) at $2\theta = 15°$ [24]. After ball milling with carbon for just 6 h and then heated at 450 °C for 3 h, the FSDP feature of the red P disappeared. Instead, a distinct peak appeared at $2\theta = 23°$ at the same time, suggesting that amorphous phosphorus is homogeneously distributed in the framework of the porous carbon, which is in agreement with previously reported amorphous red phosphorus [18], leading to the improved electrical conductivity. The phosphorus elemental mapping images (Fig. 3d) clearly demonstrate the conclusions.

Figure 3 shows the representative scanning electron microscopy (SEM) and mapping image of the P@C sample. As can be seen in Fig. 3a, c, the carbon is composed of large numbers of irregular sheet, just like the schematic inserted in Fig. 3c. To gain the intrinsic structure of the carbon, the enlarged figure in red rectangle is displayed in Fig. 3b. It is found that the present P@C sample takes on obvious plate-like particle morphology (Fig. 3b, c). Hence, this result well matched with the H3 loop of type IV that BET test before. Figure 3d, e shows the carbon and phosphorus elemental mapping images separately and clearly demonstrates that most of the phosphorus is homogeneously distributed in the framework of the carbon. In short, SEM and mapping images of the amorphous red phosphorus/carbon composite indicate that phosphorus and carbon are homogeneously mixed together on a nanoscale, resulting in improved electrical conductivity.

The Raman spectrum of slit-shaped porous carbon exhibits characteristic peaks of G- and D-bands from graphene layers, while the spectrum of crystalline phosphorus shows several well-defined peaks in the 300–500 cm^{-1} region (Fig. 4). The G-band (ca. 1588 cm^{-1}) in the carbon spectrum can be assigned to a strong C-C stretching mode, while the D-band (ca. 1350 cm^{-1}) is attributed to breathing mode of six-membered rings. This mode has been linked to the break of symmetry occurring at the edges of graphite sheets which originated from some kind of imperfection and disorder, such as defects, discontinuity in crystallites, and stacking disorder in the crystal structure of graphite [25]. The Raman intensity and wavenumber of both D- and G-bands are modified in the spectra of the composites, indicating a charge transfer to or from graphite sheets [26]. Additionally, by comparing the change of wavenumber between D-bands and G-bands, the redshift of the G-band from 1588 to 1571 cm^{-1} can then be assigned to an electron transfer in the p antibonding band of the graphite, leading to both weakening of the C-C bond and increase of the C-C distance. This electronic transfer is a proof of the interactions between the carbon matrix and the dispersed phosphorus in the composite materials [16].

The thermal behavior of P@C composite was investigated by thermogravimetry/differential scanning calorimetry (TG/DSC) in a nitrogen atmosphere, and the results are shown in Fig. 5. In DSC curve, there are three distinct
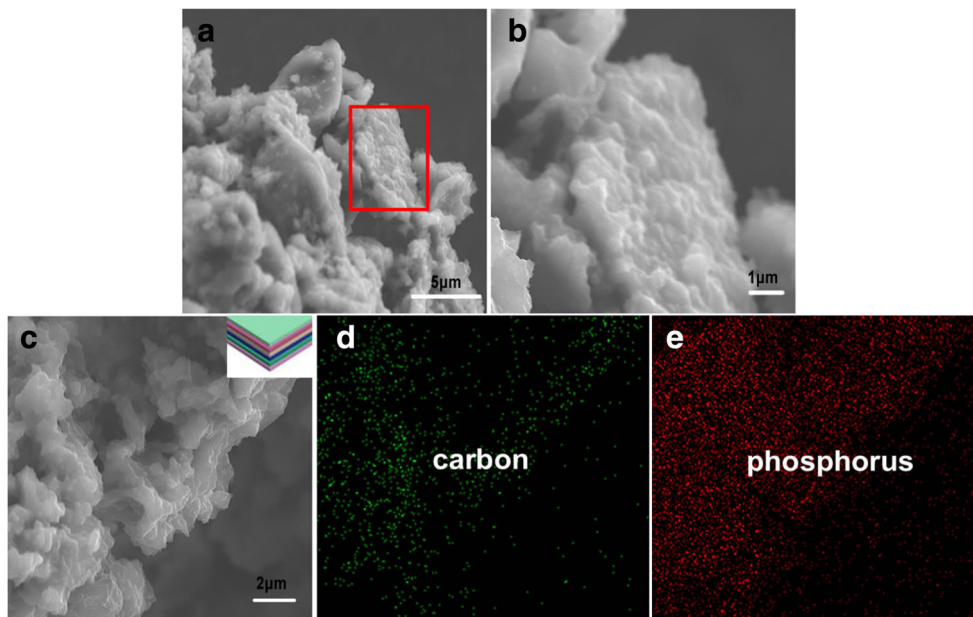
Table 1 BET surface area, DFT pore volume, and micropore volume of the slit-shaped pores carbon

Element	Surface area ($m^2\ g^{-1}$)	Pore volume (cc g^{-1})	Micropore volume (cc g^{-1})
Carbon	1158	1.061	0.406
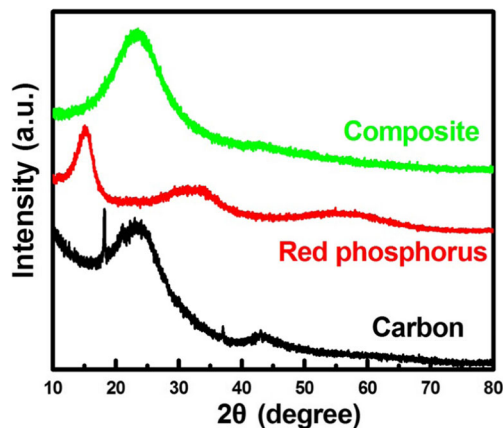
Fig. 2 X-ray diffraction patterns of carbon, red phosphorus and composite

Fig. 3 **a**–**c** SEM image of the phosphorus/carbon composite; **d**, **e** phosphorus elemental mapping images


endothermic peaks assigned to the sublimation of physically absorbed water and red phosphorus, corresponding to the three weight loss process in TG, respectively. In detail, the first weight loss at 30–100 °C is mainly due to desorption of physically absorbed water, showing the endothermic peak at 87 °C. The second weight loss at 200–300 °C can be attributed to the sublimation of red phosphorus in the micropore, which is accompanied by a little endothermic peak at 275 °C in DSC curve. The last and sharp weight loss at 450–650 °C corresponds to the red phosphorus sublimation in mesoporous. It shows a sharp exothermic peak at 545 °C, whereas red phosphorus shows a sharp weight loss at about 416 °C, the temperature at which red phosphorus sublimes, indicating that phosphorus in the composite is more stable than elemental phosphorus [18]. Considering no obvious weight loss of carbon at 800 °C in a nitrogen atmosphere, the weight loss of composite is mainly from sublimation of red

phosphorus. By analyzing these phenomena, the high adsorption strength between phosphorus and carbon matrix is proved, and it might be chemical interaction. These results are matched with XRD and Raman data. Therefore, the thermal stability of the composite is expected to be sufficient for battery applications. In addition, the content of phosphorus in the "filled" carbon is about 47.2 wt% through the TG curve. Specially, there is ~15.8 wt% of phosphorus in micropore and others in mesopore. In other words, the content of phosphorus in micropore accounts for 33.5 % of the total phosphorus, which is slightly smaller than the volume ratio. Considering that the micropore whose diameter is less than 1 nm is not available, the result is reasonable.

Figure 6a shows charge/discharge curves of the composite at the initial discharge process and the second cycle process. The composite/Li cell was assembled and tested for its electrochemical behavior at the current density of 100 mA g^{-1}.
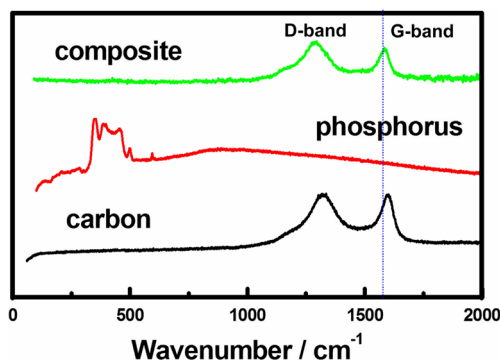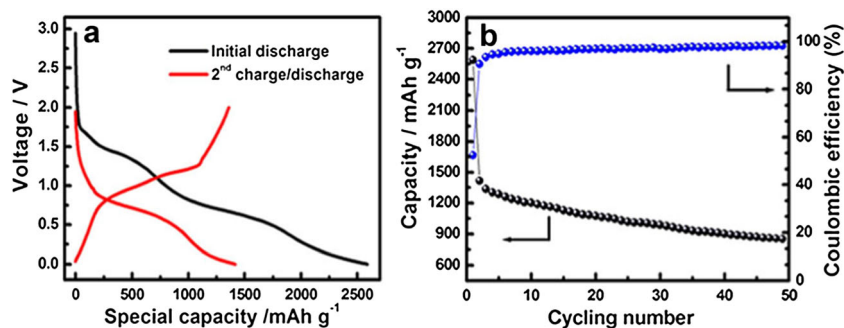

Fig. 4 Raman spectra of carbon, red phosphorus, and phosphorus/carbon composite
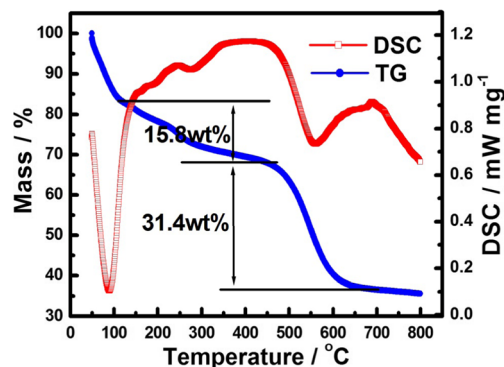
Fig. 5 TG/DSC curve of phosphorus/carbon composite in argon atmosphere

Fig. 6 Charge–discharge profiles of the initial two cycles (**a**), cycle performance, and coulombic efficiency (**b**) of the phosphorus/carbon composite at a current density of 100 mA g^{-1}

During the first discharge, the discharge voltage curve shows the insertion of 2588 mAh of lithium ion per gram composite in two processes at 1.45 and 0.75 V. Upon recharge, up to 2.0 V, 1359 mAh of lithium ion can be removed out, leading to an initial coulombic efficiency of 53 % and initial irreversible capacity of 1229 mAh g^{-1}. This phenomenon occurred as a probable result of phosphorus on the external surface where irreversible reaction happened. The coulombic efficiency of pure phosphorus is too low (Fig. S3ax). Another possible reason is derived from carbon materials. Based on charge/discharge curves of pure carbon, carbon delivers the first discharge capacity of 761 mAh g^{-1} during the first discharge and presents cycling capacities of about 295 mAh g^{-1} in the following cycles (Fig. S3b). To further express the unique superiority of our phosphorus-slit-shaped porous carbon, the cycling performance of composite is tested at a current of 100 mA g^{-1} for 50 cycles in the voltage range of 0 to 3.0 V versus Li/Li$^+$ (Fig. 6b). The phosphorus composite shows the capacity retention over 60 % from the second cycle to 50th cycle. The average capacity degradation rate is less than 0.8 % per cycle excluding the first discharge process. The composite presents an initial coulombic efficiency of 53 %, which is a weak point. Fortunately, the coulombic efficiency increases to 95 % after five cycles, implying less consumption of electrolyte and lithium. And the composite has a high coulombic efficiency value of over 99 % after 50 cycles. Compared with others' work (Table S1), the red phosphorus composite is a potential candidate anode material for lithium-ion batteries. In addition, comparing with electrochemical performance of other carbon which has the same pore volume but different size distribution, we claim that the size distribution plays an important role in adsorbing phosphorus and electrochemical performance (Fig. S4).

4. Conclusions

In summary, we have proposed a research direction to develop phosphorus composite material from carbon structure, in which the carbon materials served as the electronically conductive support matrix. Slit-shaped porous carbon has its unique advantages of pore structure for phosphorus-carbon composite and is worthy of further studying. Furthermore, we have demonstrated its electrochemical performance as an anode material for lithium-ion batteries. This composite shows initial capacity of 2588 mAh g^{-1} and an excellent coulombic efficiencies of ~99 % after 50 cycles with high reversible capacity. Thus, the excellent electrochemical performance makes it a promising candidate for lithium-ion batteries, considering with the natural abundance and environmental friendliness of the phosphorus element.

References

1 Arico AS, Bruce P, Scrosati B, Tarascon J-M, van Schalkwijk W (2005) Nanostructured materials for advanced energy conversion and storage devices. Nat Mater 4:366–377

2 Maier J (2005) Nanoionics: ion transport and electrochemical storage in confined systems. Nat Mater 4:805–815

3 Bruce PG, Scrosati B, Tarascon J-M (2008) Nanomaterials for rechargeable lithium batteries. Angew Chem Int Ed 47:2930–2946

4 C.-X. Zu, H. Li, (2011) Thermodynamic analysis on energy densities of batteries. Energy & Environmental Science 4:2614–2624.

5 Lou XW, Wang Y, Yuan C, Lee JY, Archer LA (2006) Template-free synthesis of SnO2 hollow nanostructures with high lithium storage capacity. Adv Mater 18:2325–2329

6 Idota Y, Kubota T, Matsufuji A, Maekawa Y, Miyasaka T (1997) Tin-based amorphous oxide: a high-capacity lithium-ion-storage material. Science 276:1395–1397

7 Cui Y, Zhong Z, Wang D, Wang WU, Lieber CM (2003) High performance silicon nanowire field effect transistors. Nano Lett 3:149–152

8 Cui L-F, Yang Y, Hsu C-M, Cui Y (2009) Carbon−silicon core−shell nanowires as high capacity electrode for lithium ion batteries. Nano Lett 9:3370–3374

9 Mitra S, Poizot P, Finke A, Tarascon JM (2006) Growth and electrochemical characterization versus lithium of Fe3O4 electrodes made by electrodeposition. Adv Funct Mater 16:2281–2287

10 Fang S, Tang Y, Tai X, Yang L, Tachibana K, Kamijima K (2011) One ether-functionalized guanidinium ionic liquid as new electrolyte for lithium battery. J Power Sources 196:1433–1441

11 Nishijima M, Tadokoro N, Takeda Y, Imanishi N, Yamamoto O (1994) Li deintercalation intercalation reaction and structural change in lithium transition metal nitride, Li7MnN4. J Electrochem Soc 141:2966–2971

12 Shodai T, Okada S, Tobishima S-i, Yamaki J-i (1996) Study of Li3
    −xMxN (M: Co, Ni or Cu) system for use as anode material in
    lithium rechargeable cells. Solid State Ionics 86–88, Part 2:785–789

13 Woo S-g, Jung J-H, Kim H, Kim MG, Lee CK, Sohn H-J, Cho BW
    (2006) Electrochemical characteristics of Ti–P composites prepared
    by mechanochemical synthesis. J Electrochem Soc 153:A1979–
    A1983

14 Kim Y-U, Cho BW, Sohn H-J (2005) The reaction mechanism of
    lithium insertion in vanadium tetraphosphide: a possible anode ma-
    terial in lithium-ion batteries. J Electrochem Soc 152:A1475–A1478

15 Kim Y-U, Lee CK, Sohn H-J, Kang T (2004) Reaction mechanism
    of tin phosphide anode by mechanochemical method for lithium
    secondary batteries. J Electrochem Soc 151:A933–A937

16 Marino C, Debenedetti A, Fraisse B, Favier F, Monconduit L (2011)
    Activated-phosphorus as new electrode material for Li-ion batteries.
    Electrochem Commun 13:346–349

17 Park CM, Sohn HJ (2007) Black phosphorus and its composite for
    lithium rechargeable batteries. Adv Mater 19:2465–2468

18 Wang L, He X, Li J, Sun W, Gao J, Guo J, Jiang C (2012) Nano-
    structured phosphorus composite as high-capacity anode materials
    for lithium batteries. Angew Chem Int Ed 51:9034–9037

19 Kim Y, Park Y, Choi A, Choi N-S, Kim J, Lee J, Ryu JH, Oh SM,
    Lee KT (2013) An amorphous red phosphorus/carbon composite as
    a promising anode material for sodium ion batteries. Adv Mater 25:
    3045–3049

20 Wang Y, Xiong R, Dong L, Hu A (2014) Synthesis of carbon
    nanomembranes through cross-linking of phenyl self-assembled
    monolayers for electrode materials in supercapacitors. Journal of
    Materials Chemistry A 2:5212–5217

21 K.S.W. Sing, D.H. Everett, R.A.W. Haul, L. Moscou, R.A. Pierotti,
    J. Rouquerol, T. Siemieniewska, Reporting physisorption data for
    gas/solid systems, Handbook of Heterogeneous Catalysis, Wiley-
    VCH Verlag GmbH & Co. KGaA2008.

22 Yang X, Zhang L, Zhang F, Huang Y, Chen Y (2014) Sulfur-
    infiltrated graphene-based layered porous carbon cathodes for
    high-performance lithium–sulfur batteries. ACS Nano 8:5208–5215

23 Hulicova-Jurcakova D, Puziy AM, Poddubnaya OI, Suárez-García
    F, Tascón JMD, Lu GQ (2009) Highly stable performance of
    supercapacitors from phosphorus-enriched carbons. J Am Chem
    Soc 131:5026–5027

24 Zaug JM, Soper AK, Clark SM (2008) Pressure-dependent struc-
    tures of amorphous red phosphorus and the origin of the first sharp
    diffraction peaks. Nat Mater 7:890–899

25 Baddour-Hadjean R, Pereira-Ramos J-P (2010) Raman
    microspectrometry applied to the study of electrode materials for
    lithium batteries. Chem Rev 110:1278–1319

26 Chan CT, Ho KM, Kamitakahara WA (1987) Zone-center phonon
    frequencies for graphite and graphite intercalation compounds:
    charge-transfer and intercalate-coupling effects. Phys Rev B 36:
    3499–3502